Preprints of the 21st IFAC World Congress (Virtual)
Berlin, Germany, July 12-17, 2020

Design of a Capacitance Sensor for Human Intention Detection of Daily Living Activities

Pyeong-Gook Jung, Yacine Amirat, and Samer Mohammed *

* *Laboratory of Images, Signals and Intelligent Systems, University of Paris-Est Créteil, Créteil 94000, France, (e-mail: pgjung.lissi@gmail.com, amirat@u-pec.fr, samer.mohammed@u-pec.fr).*

Abstract: As many countries enter an aging society, the demand of wearable robots are increasing. To apply wearable robots in daily life, the intention recognition of the wearers is of great important. Although this research field has been extensively studied in the last decade, still the physical intention recognition based approaches are facing different challenges and in particular when used in assistive and rehabilitation scenarios. In this paper, we propose to monitor muscular activities of the shank and movement of the ankle joint by using capacitance sensors. The proposed capacitance sensor monitor the electrodermal activities under the human skin. The human skin has capacitance when an external current is applied and muscular activities can change the capacitance. To verify the proposed capacitance sensor, the human joint angle was measured by two inertial sensors and the capacitance sensor on the shank at once. The electromyogram(EMG) signals were also compared to verify the performance of the intention detection device based on the capacitance sensors.

Keywords: Intention recognition, wearable robot, exoskeleton robot, electromyography, mechanomyography, human-machine interface, human-robot interface, human mechatronics

1. INTRODUCTION

Every year an increasing number of people are diagnosed with disabilities that prevent them from performing basic daily living activities such as walking, stairs ascent/descent, ramps ascent/descent, etc. Around 15% of the world population lives with a certain form of disability according to the World Health Organization; among them 2%-4% are facing important difficulties while performing daily activities. Patients suffering from gait pathologies may either have total or partial loss of lower limbs muscle forces and thus are respectively unable to initiate a movement or moving their affected limbs within limited ranges of motion.

Facing gait pathologies effects range from conventional therapy, to the use of functional electrical stimulation (FES) and passive/active orthosis solutions known also as wearable robotics (Coste et al. (2014), Peckham, P. Hunter and Knutson, Jayme S. (2005)). The use of active wearable robots provide quantified assistance and could potentially adapt the intensity of the robot-side assistance with respect to the required efforts from the wearer following a pre-defined rehabilitation protocol. Recently, the exoskeleton robots for the complete paraplegia caused by spinal cord injury (SCI) have been developed and their performances were shown at Cybathlon 2016. In this competition, ReWalk, IHMC X1 and WalkON Suit(Choi, J., Na, B., Jung, P.-G., Rha, D., and Kong, K. (2017)) showed their potentials by successfully performing five of six tasks: 1) Sitting down and standing up; 2) slalom; 3) ramp up and down; 4) rough terrain; 5) tilted path and 6) stairs up and down. However, intention recognition system has been developed to be use such robots in daily life.

One way of intention recognition is to detect signal propagation through the central nerve system (CNS) of the human body. Neurons, which are the main components of the CNS, exchange information to achieve a desired movement. During CNS information transmission, electrical potentials change due to depolarization and repolarization of ions in the human body. An EMG or electroencephalogram (EEG) measure such changes of potentials to recognize muscular activities. Depending on the attached positions, these sensors are called EMG or EEG respectively.

In the last decade, these sensors have been extensively used in control strategies of wearable robots. (McDaid et al. (2013); He et al. (2018)) proposed EEG-based control strategies for exoskeleton. For the HAL-3 and HAL-5 systems which are lower limbs exoskeleton devices developed Cyberdyne, EMGs are used to measure the muscular activities as input to the actuator controllers(Kawamoto and Sankai (2002); Kawamoto et al. (2003)). Although measuring signal propagation is the most noteworthy approach to detect the wearer's intention since it reflect the direct intention of the wearers, there are some limitations and challenges to overcome. Since the potential level of signal propagation is less than $100mV$(Kolb and Whishaw (2009)), additional signal processing operations are required to ensure an accurate envelop curve of muscle activation such as differential amplifier, low-pass filter or notch filter(Mills (1982)). Furthermore, to reduce the effect of the skin resistance, the epidermis should be regularly cleaned otherwise the EEG and EMG electrodes should be of invasive type to guarantee satisfactory performances of the sensors(Basmajian (1973)).

For these reasons, (Yamamoto et al. (2002)) designed muscle hardness sensor system to measure the force generated by the muscles. A load cell is implemented between two plates to measure swelling of the skin caused by muscle contraction. However, the load cell is relatively expensive with respect to other sensors and it needs additional circuits. (Jung et al. (2015)) pro-

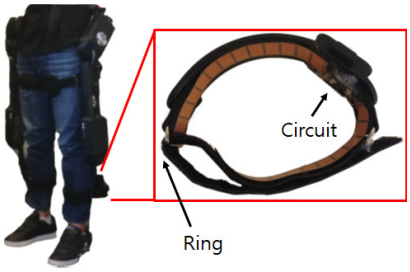

Fig. 1. A cuff of wearable robot with the proposed capacitance sensor

posed, in a previous study, a pressure based mechanomyogram (pMMG) system to measure the muscular activities with air-bladder and pressure sensors. The pMMG system shows robust performance with respect to noise. However, the pMMG system suffers from a large volume of the air-bladder.

In this paper, a capacitance sensor based system for muscular activities monitoring is proposed to recognize intention of a human wearing a lower limb exoskeleton. The muscles in the shank are measured by the proposed system to recognize the ankle joint movement because the ankle plays an important role in advancing the body weight (Perry et al. (1992)).

When an external current is applied to the human skin, the cell membranes are able to store the electrical charge and act as capacitors. The capacitance sensors monitor the electrodermal activities (EDA) and measure the changes in length caused by muscle contraction. Since the human has relatively enough capacitance with respect to the applied current, the grounds of both the circuit and the human do not need to be connected. Therefore, the electrodes can be applied without contact with the human. Due to their thickness the proposed capacitance sensor system can be applied inside the strap of a wearable robot without affecting their performances, which is very practical for wearability. Furthermore, the proposed system monitors smaller segment on the bigger segment, e.g the proposed system attached on the shank measures movement of the foot. It leads to measure the movement of two joints in one joint. To monitor EDA, thin and non-contact electrode is used inside the cuff of lower wearable robot(Angel Suit) as shown in Fig. 1. The shank muscle activity of three healthy subjects during level walking (LW), stairs up (SU), stairs down (SD), and ramp up (RU) for each step are studied to show the performance of the proposed capacitance sensor. The rest of the paper is organised as follows: Section II describes principal of the proposed capacitance sensor. Section III shows performance of the proposed capacitance sensor. Section IV presents comparison with EMG sensors.

2. PRINCIPAL OF THE PROPOSED CAPACITANCE SENSOR

2.1 Human Skin Capacitance Properties

The skin can be largely divided into three layers upon the vertical direction. In the epidermal layer which is the outermost layer, the cells are keratinized and regarded as dead passive cells. On the other hand, the cells of nerve, muscle, and glands such as sweat glands, blood capillaries, and lymphatic duct, which are located in the dermal and hypodermal layers are active as these membranes present a resting charge. The active membranes also show capacitive properties when they are stimulated (Boucsein (2012)).

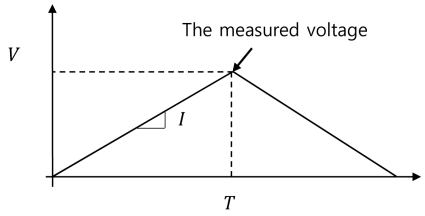

Fig. 2. The capacitance measurement process

The density of these properties remains unchanged if the skin length does not change, meaning that there is not muscular contraction under the skin. However, the contraction caused by muscular activities changes skin length consequently and changes the capacitance property density in the skin. When a motion occurs, *eccentric* contraction and *concentric* contraction occur together. *eccentric* contraction lengthens the muscles and the skin while *concentric* contraction makes the length of the muscle and skin(Huxley (1969)). For example, during ankle dorsiflexion, the skin length on the anterior of the shank is shortened, while the skin length on the posterior of the shank is lengthened.

Due to the changes of the skin length, the density of the capacitive properties in the skin changes as well. As a result of *eccentric* contraction, the density of capacitive properties increases and leads to an increasing capacitance. On the other side, the density of capacitive properties decreases as a result of *concentric* contraction and it leads to a decreasing capacitance.

2.2 Capacitance Measurement

To measure the EDA, the capacitance sensor, *MPR*121 which is produced by Freescale Semiconductors Co., was utilized. *MPR*121 can measure the capacitance of twelve electrodes using the multiplexed sensing inputs and contains an analog to digital converter (ADC) with a 10*bits* resolution. The capacitance sensor measures the capacitance by charging the constant electric current for a transient time due to the fact that a capacitor has a resistance with respect to the frequency of the applied voltage. Since the sensor charges the constant electric current, the relationship between the amount of the electric charge and the current can be expressed as follows (MPR121 (2010)).

$$q = IT \tag{1}$$

where q is the quantity of electric charge, I is the constant current, and T is the charging time which is constant. I and T are determined by the registry value of the *MPR*121. Therefore, the capacitance, C, is calculated as follows.

$$C = \frac{q}{V} = \frac{IT}{V} \tag{2}$$

where V is the voltage of each electrode. The capacitance sensor measures the voltage to calculate the capacitance. Therefore the output of ADC is as follows.

$$V = \frac{IT}{C} \tag{3}$$

The above process is described in Figure 2.

The change of the density leads to a capacitance change as mentioned above. The increase in density caused by a *concentric* contraction leads to a capacitance increase. As a result, the measured voltage from capacitance sensor decreases.

Fig. 3. The electrode of the proposed capacitance sensor

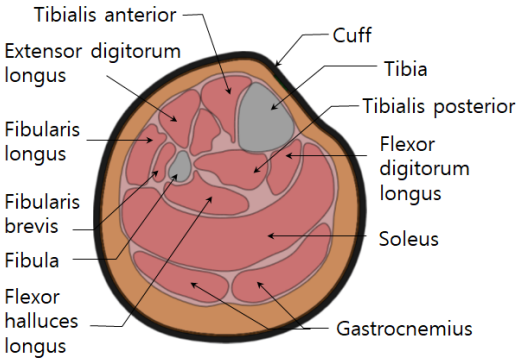

Fig. 4. The cross-section of the shank

2.3 Hardware Description

The system consists of a cuff of wearable robot, electrodes and a circuit. The size of the electrode is $11mm \times 30mm$ and the thickness of the electrode is $0.2mm$. Since the electrode is very thin, the flexibility of the electrode is appropriate for a wearable device. The number of electrode is twenty four. Therefore, the number of channels to measure the EDA of the shank is also twenty four. The circuit consists of a microprocessor unit (MCU), an inertial measurement unit (IMU), RS232 to universal asynchronous receiver/transmitter (USART) interface and two capacitance sensors. Since the MCU has a direct memory access for Inter-Integrated Circuit (I2C) for capacitance sensor, Serial Peripheral Interface (SPI) for IMU and RS232 communications, MCU is mainly used for signal processing and intention recognition. Thus, the sampling rate of the proposed capacitance sensor can be up to 100Hz in real-time. IMU which consists of three-axis accelerometer, gyroscope, and magnetometer was implemented to measure the angle of the shank. To improve durability, the entire circuit was implemented on a printed circuit. Furthermore, the electrodes were also manufactured in a flexible printed circuit board (see Figure 3). Therefore, the capacitance of the circuit was fixed which increases the reliability of the measurement.

2.4 Anatomy of the Human Shank

Since the muscles to contract the ankle joint are placed in the shank, the proposed capacitance sensor is placed on the shank. Figure 4 shows the cross-section of the human shank. As shown in Fig. 4, the different muscles make the system redundant over the ankle and toes joints. As a result when one motion occurs, several muscles rather than just one are activated and interact together to generate smooth motion of the ankle joint. For example, dorsiflexion occurs when *tibialis anterior* and *extensor hallucis* are *concentric* contracted while *tibialis posterior*, *fibularis longus*, *fibularis brevis*, *flexor halluces longus*, *gasrocnemius* and *soleus* are *eccentric* contracted. Further detail on the role of each muscle is shown in Table 1.

Table 1. Role of the muscles

Joint	Motion	Muscle
Toe	Flexion	*Flexor digitorum longus*(FDL) *Flexor halluces longus*(FHL)
	Extension	*Extensor digitorum longus*(EDL) *Extensor hallucis longus*(EHL)
Ankle	Dorsiflexion	*Extensor hallucis longus* *Tibialis anterior*(TA)
	Plantarflexion	*Fibularis longus*(FL) *Fibularis brevis*(FB) *Flexor halluces longus* *Gastrocnemius*(GAS) *Soleus*(SOL)
	Inversion	*Tibialis anterior* *Tibialis posterior*(TP)
	Eversion	*Fibularis longus* *Fibularis brevis*

Table 2. Locations of the electrodes

Muscles	Electrode number
GAS	1-3, 18-22
SOL	5-6, 13-16
FL	7-8
EDL	9-10
TA	12
N/A	4, 11, 17, 23, 24

3. PERFORMANCE OF THE PROPOSED CAPACITANCE SENSOR

3.1 Experimental Setup

To check the feasibility of the proposed capacitance sensor, two experiments were conducted. The first one was to measure the ankle joint angle and the second one was to measure the profile of the signal measured by the proposed capacitance sensor place at the shank level during gait cycle for level walking.

The ankle joint angle was measured by using two IMUs manufactured by (Xsens). To measure the shank angle, the IMU in the proposed capacitance sensor was used. The other IMU was attached on the foot. Since both of the IMUs have the same sampling rate, i.e., 100Hz, it is possible guarantee signal synchronisation.

To quantify the voltage output measured by the proposed capacitance sensor, the subject was asked to conduct level walking. In order to extract the measurements of proposed capacitance sensor for each gait cycle, an IMU-based gait detection algorithm was utilized (Huo et al. (2018)). The results of the experiments were analyzed based on the role of each muscles while walking as described in the literatures (Townsend et al. (1978); Perry et al. (1992)).

Fig. 5 shows the locations of the electrodes and circuit. Since there is no muscle on the tibia, the circuit of the proposed capacitance sensor is placed on the tibia. Ring of the cuff was place on the *gastrocnemius*,to fasten the system since there is enough space to measure the activity of the *gastrocnemius*. The detailed locations of the electrode are described in Table 2. Channel number 23 and 24 are extra channels for the thick shank.

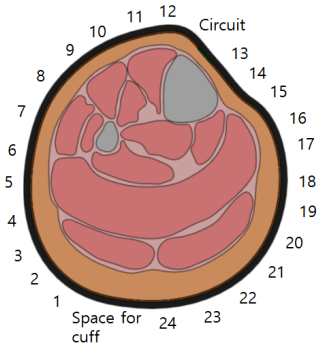

Fig. 5. Locations of the circuit and electrodes

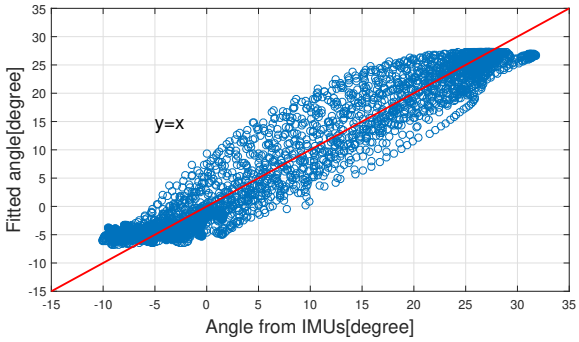

Fig. 6. The experimental result for comparison with IMU

3.2 Linearity of the Proposed Capacitance Sensor Joint Angle

The subject was asked to perform the dorsiflexion and plantarflexion of the ankle thirty times. To reduce the influence from other motions such as inversion and eversion, the ankle joint was restricted by using an Ankle-Foot orthosis.

The angles measured by the two IMUs were calculated based on the inner product of each joint vector as follows.

$$V_{initial} = \begin{bmatrix} 0 \\ 0 \\ 1 \end{bmatrix} \tag{4}$$

$$V_{Shank} = R_{Shank} V_{initial} \tag{5}$$

$$V_{Foot} = R_{Foot} V_{initial} \tag{6}$$

$$\theta = \arccos \frac{V_{Shank} \cdot V_{Foot}}{\|V_{Shank}\| \, \|V_{Foot}\|} \tag{7}$$

where R is a three-dimensional rotation matrix measured by IMUs, and $V_{initial}$ is a unit vector. V_{Shank} and V_{Foot} represent segment vectors with respect to the foot and shank segments. θ denotes the ankle joint angle.

To measure the ankle dorsiflexion and plantarflexion angles, the most significant signals, i.e., the measurement of the *gastrocnemius*, were curve-fitted to a quadratic function. Since the signals of the proposed capacitance sensor are capacitance, the relationship between each channel are parallel capacitors. Therefore, the activities of the relatively important muscles which are calculated as the summation of multiple channels. For this reason, the curve-fitted angle was calculated by the summation of the signals of 1 to 3 and 18 to 22 channels in Fig. 5. The relationship between fitted ankle joint angle from proposed system and the measurement of the *gastrocnemius* was represented by the following quadratic function.

$$\theta_{Gas} = -0.078M^2 + 1.70M + 408.56 \tag{8}$$

where θ_{Gas} is fitted angle and M is summation of the signals of 1 to 3 and 18 to 22 channels. The correlation coefficient between the measured angle and curve-fitted angle from the proposed capacitance sensor was 0.9741 (see Figure 6).

3.3 Signal Profile While Walking

Each gait cycle (GC) can be largely divided into two phases: the swing phase and the stance phase. Stance phase is subdivided into initial contact (IC), loading response (LR), mid stance (MSt), and terminal stance (TSt). Swing phase could be subdivided into pre-swing (PS), initial swing (IS), mid swing (MSw), and terminal swing (TSw) (Perry et al. (1992)).

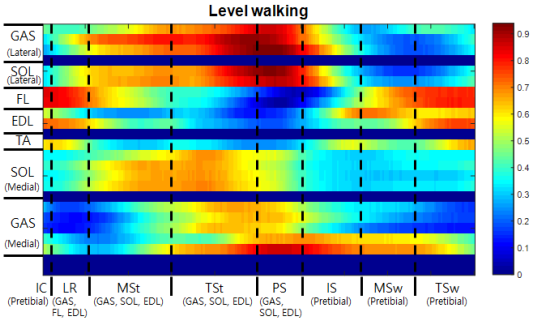

Fig. 7. The signal profile while level walking

During IC which is the first 2% of the GC, the *pretibial* muscles in shank are activated to preserve progression and absorb the ground impact. During LR which is 2∼10% of the GC, a plantar flexion torque is generated by the GAS, FL, and FB for rapid loading of the body weight while TA and EDL starts activation to decelerate an excessive dorsiflexion. In MSt phase which is 10∼30% of the GC, the SOL contributes for the progression and stability of the human body. In this phase, GAS is also activated. However, there is a certain delay compared to the SOL activation (Sutherland (1966)). These two muscles keep contracting until TSt which is 30∼50% of GC. In PS phase which is 50∼60% of GC, the SOL and GC start deactivation and TA is contracted to decelerate the rate of foot fall. In swing phase, *pretibial* muscles are activated to retain clearance from the floor and compensate the gravity of the foot.

Fig. 7 shows the profile measured by the proposed capacitance sensor. The subject was asked to walk on the flat plain for 20 steps. The muscular activities according to the gait phase are briefly described in the figure. The signals from the proposed capacitance sensor are normalized with respect to the maximal voluntary contraction. The signals of the electrodes which have interference between two muscles or the electrodes of muscle-less part were set to zero by post-processing. The muscular activities are represented by color of the area. Red area means the muscle is in maximal contraction and blue area means the muscle is in the neutral posture.

4. COMPARISON WITH EMG SENSORS

4.1 Experimental Setup

Because the EMG signals reflect the signal propagation in the human body to contract the muscles, the performance of the proposed system was verified with EMG sensors. The TA,

Table 3. Information of the subjects

Subject	Age	Height (cm)	Weight (kg)
A	30	170	63
B	26	190	71
C	28	178	64

GAS, and SOL muscles were measured by EMGs manufactured by (Delsys). The location of the EMG sensor modules were determined based on the anatomy and adjusted to take into account individual differences. The sampling frequency of EMG sensor is 1kHz.

The most common terrains encountered in urban environment are flat, stairs, and ramps. To implement the proposed capacitance sensor in daily life, the proposed capacitance system was used on three terrains. Subjects were asked to walk on the flat plain, stairs descend, stairs ascend and ramp up on a treadmill with 3, 6, and 9 degrees of incline angle. In this chapter, the profiles of the muscular activities measured by the proposed capacitance sensor are compared with EMG sensors for three healthy subject and the peak activated timing for three muscles in gait cycles. The information of the three subjects are described in Tab. 3.

4.2 Signal Processing

The default channel arrangement is shown in Fig. 5. Since the proposed system was installed inside of wearable robot's cuff, i.e. rigid body, the proposed system could be placed on the same position for each experiment. However, there can be differences for each person. To address this problem, the correlations of between two adjacent electrodes and the results of EMG sensors were calculated. For example, the correlations between electrode number 10-14 and EMG signal from the TA muscle for whole experiments were calculated to find the exact locations of the electrodes.

To get an envelop curve from the EMG signal, the EMG signals were processed by three steps. First, the EMG signals were rectified since the measured EMG signals are difference between two electrodes of EMG sensor. For the second and third steps, the EMG signals were filtered by high-pass filter and low-pass filter which have 100Hz and 3Hz of cutoff frequency, respectively. Since the sampling frequency of the proposed system is 100Hz as mentioned above, the processed signal of EMG sensor were re-sampled and normalized with the maximal voluntary contraction value (%MVC).

To analyze for each gait cycle, the signals from the EMG sensors and the proposed system were extracted for each gait cycle by the swing detection algorithm as mentioned in Chapter 3. The measurements from the proposed system were fitted with first-order polynomial function to compare with EMG signal.

4.3 Experimental Results

Fig. 8 shows the experimental results. The red line shows the measurements from the EMG sensor and the black line shows the measurements from the proposed system. The dashed blue line shows the result of the swing detection algorithm. To analyze statistically, the measurements were extracted for each step.

Fig. 9 shows the average of measurements for each step. The red line and black line are the average of measurements from the EMG sensor and the proposed system more than 100 steps, respectively. The dashed line represents the standard deviation of each result. The x-axis of the figure represents the gait duration in percentage of the gait cycle and the y-axis of the figure is %MVC.

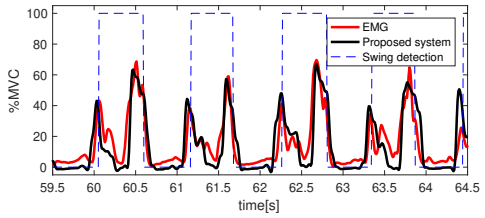

Fig. 8. The experimental results while level walking in time domain

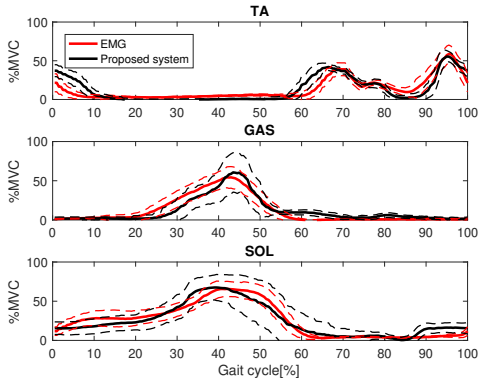

Fig. 9. The signal profile while level walking during gait

To quantitatively analyze two signals, correlation was introduced. Table 4 shows the results of the experiments. The value represents similarity between two signals. If the signals are the same, the correlation is 1 and if the signals have no relation, the correlation is 0. In other words, if the correlation is 0.9, it means that the two signals are 90% identical. As shown in Table 4, all results show more than 70% similarity.

To identify human intention, it is important when the muscles are most activated during the gait cycle. Fig. 10 shows error of the most activated duration between two systems. Although the SOL error of subject C shows larger than 20% of gait cycle, the standard deviation of the error was less than 2%. It means the measurements from the proposed system shows periodic performance.

5. DISCUSSION

In this paper, muscular activity monitoring system based on capacitance sensors. EDA is monitored to measure muscular activities. To check feasibility of the proposed capacitance sensor for wearable robots, the electrodes of the proposed capacitance sensor has been implemented inside of the cuff of wearable robots. The performance of the proposed capacitance sensor is verified with IMUs. The curve-fitted angle shows the linearity of 0.9741 with respect to the angles provided by IMUs. The profiles of the proposed capacitance sensor while normal walking was also verified with EMG reference. For each gait cycle, the muscular activities measured by the proposed capacitance sensor shows the same trends as the EMG reference.

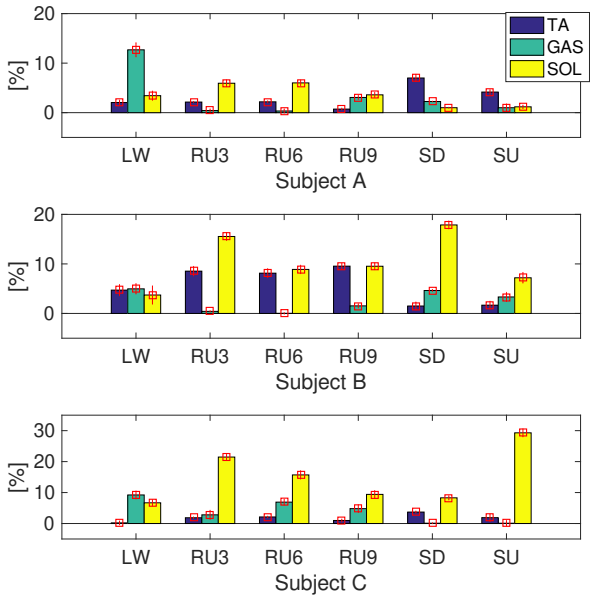

Fig. 10. The error of the most activated duration between two systems

Table 4. The correlation between the EMG and proposed system during the whole experiment

Subject	States	TA	SOL	GAS
A	LW	0.85	0.92	0.96
	RU3	0.87	0.94	0.95
	RU6	0.88	0.96	0.97
	RU9	0.87	0.96	0.97
	SD	0.83	0.87	0.88
	SU	0.92	0.75	0.90
	Average	0.87	0.90	0.94
B	LW	0.85	0.71	0.78
	RU3	0.86	0.76	0.86
	RU6	0.82	0.75	0.81
	RU9	0.86	0.76	0.73
	SD	0.75	0.84	0.86
	SU	0.95	0.88	0.85
	Average	0.84	0.78	0.82
C	LW	0.87	0.96	0.92
	RU3	0.78	0.89	0.94
	RU6	0.81	0.93	0.95
	RU9	0.73	0.93	0.97
	SD	0.86	0.86	0.84
	SU	0.85	0.80	0.81
	Average	0.82	0.90	0.91

To utilize the proposed capacitance sensor in daily life, a machine learning algorithm will be applied as a recognition algorithm. For the next step, the function in python which name is *tensor flow* will be implemented to recognize the intention of subjects of wearable robots in real-time.

REFERENCES

Basmajian, J.V. (1973). Electrodes and electrode connectors. In *New Concepts of the Motor Unit, Neuromuscular Disorders, Electromyographic Kinesiology*, volume 1, 502–510. Karger Publishers.

Boucsein, W. (2012). *Electrodermal activity*. Springer Science & Business Media.

Choi, J., Na, B., Jung, P.-G., Rha, D., and Kong, K. (2017). Walkon suit: A medalist in the powered exoskeleton race of cybathlon 2016. *IEEE Robotics Automation Magazine*, 24(4), 75–86. doi:10.1109/MRA.2017.2752285.

Coste, C.A., Jovic, J., Pissard-Gibollet, R., and Froger, J. (2014). Continuous gait cycle index estimation for electrical stimulation assisted foot drop correction. *Journal of neuroengineering and rehabilitation*, 11(1), 118.

He, Y., Eguren, D., Azorín, J.M., Grossman, R.G., Luu, T.P., and Contreras-Vidal, J.L. (2018). Brain-machine interfaces for controlling lower-limb powered robotic systems. *Journal of neural engineering*, 15(2), 021004.

Huo, W., Arnez-Paniagua, V., Ghedira, M., Amirat, Y., Gracies, J.M., and Mohammed, S. (2018). Adaptive fes assistance using a novel gait phase detection approach. In *2018 IEEE/RSJ International Conference on Intelligent Robots and Systems (IROS)*, 1–9. IEEE.

Huxley, H.E. (1969). The mechanism of muscular contraction. *Science*, 164(3886), 1356–1366.

Jung, P.G., Lim, G., Kim, S., and Kong, K. (2015). A wearable gesture recognition device for detecting muscular activities based on air-pressure sensors. *IEEE Transactions on Industrial Informatics*, 11(2), 485–494.

Kawamoto, H., Lee, S., Kanbe, S., and Sankai, Y. (2003). Power assist method for hal-3 using emg-based feedback controller. In *SMC'03 Conference Proceedings. 2003 IEEE International Conference on Systems, Man and Cybernetics. Conference Theme-System Security and Assurance (Cat. No. 03CH37483)*, volume 2, 1648–1653. IEEE.

Kawamoto, H. and Sankai, Y. (2002). Power assist system hal-3 for gait disorder person. In *International Conference on Computers for Handicapped Persons*, 196–203. Springer.

Kolb, B. and Whishaw, I.Q. (2009). *Fundamentals of human neuropsychology*. Macmillan.

McDaid, A.J., Xing, S., and Xie, S.Q. (2013). Brain controlled robotic exoskeleton for neurorehabilitation. In *2013 IEEE/ASME International Conference on Advanced Intelligent Mechatronics*, 1039–1044.

Mills, K.R. (1982). Power spectral analysis of electromyogram and compound muscle action potential during muscle fatigue and recovery. *The Journal of physiology*, 326(1), 401–409.

MPR121 (2010). *Proximity capacitive touch sensor controller*. Freescale Semiconductors. Rev. 4.

Peckham, P. Hunter and Knutson, Jayme S. (2005). Functional electrical stimulation for neuromuscular applications. *Annual Review of Biomedical Engineering*, 7(1), 327–360. doi: 10.1146/annurev.bioeng.6.040803.140103.

Perry, J., Davids, J.R., et al. (1992). Gait analysis: normal and pathological function. *Journal of Pediatric Orthopaedics*, 12(6), 815.

Sutherland, D.H. (1966). An electromyographic study of the plantar flexors of the ankle in normal walking on the level. *Journal of bone and joint surgery*, 48(1), 66–71.

Townsend, M.A., Lainhart, S.P., Shiavi, R., and Caylor, J. (1978). Variability and biomechanics of synergy patterns of some lower-limb muscles during ascending and descending stairs and level walking. *Medical and Biological Engineering and Computing*, 16(6), 681–688.

Yamamoto, K., Hyodo, K., Ishii, M., and Matsuo, T. (2002). Development of power assisting suit for assisting nurse labor. *JSME International Journal Series C Mechanical Systems, Machine Elements and Manufacturing*, 45(3), 703–711.